Unusual CO Adsorption Sites on Vanadium Oxide−Pd(111) "Inverse Model Catalyst" Surfaces

S. Surnev,*,† M. Sock,† G. Kresse,‡ J. N. Andersen,§ M. G. Ramsey,† and F. P. Netzer†

Institut für Experimentalphysik, Karl-Franzens Universität Graz, A-8010 Graz, Austria, Institut für Materialphysik, Universität Wien, A-1090 Vienna, Austria, and Department of Synchrotron Radiation Research, Institute of Physics, Lund University, S-223 62 Lund, Sweden

Received: October 30, 2002; In Final Form: February 20, 2003

The morphology, structure, and reactivity of vanadium oxide-decorated Pd(111) surfaces, which have been subjected to oxidation and reduction treatments, have been investigated by scanning tunneling microscopy (STM), high-resolution electron energy loss spectroscopy (HREELS), and high-resolution X-ray photoelectron spectroscopy (HR-XPS) with synchrotron radiation combined with ab initio density functional theory (DFT) calculations. Two major oxide phases form on the Pd(111) surface following the oxidation (V_5O_{14}) and reduction (s-V_2O_3) treatments; their structures have been revealed with the help of the DFT calculations. The reactive sites of both oxidized and reduced vanadium oxide/Pd(111) surfaces have been studied using the adsorption of CO as a test molecule for probing the free Pd sites. The adsorbate (C 1s) and substrate (Pd 3d) core level XPS data show that on the reduced, s-V_2O_3-decorated Pd(111) surfaces, CO occupies the same adsorption sites as on the clean Pd(111). In contrast, a new type of CO adsorption site is found on the oxidized, V_5O_{14}-covered Pd(111) surfaces that is associated with the adsorption of CO within the open (4×4) oxide lattice. The latter contains holes with six free Pd atoms per unit cell, which may be considered as a particular kind of an "adsorption pocket".

1. Introduction

In recent years, significant efforts to integrate modern surface science techniques into fundamental catalytic research have been undertaken, driven by the need to comprehend heterogeneous catalysis processes at a molecular level. Since a detailed investigation of catalytic processes is often hampered by the complex structure of the industrial catalysts, model systems have been designed and studied. Most of the work so far has involved metal nanoparticles deposited on suitable oxide supports, and excellent reviews on this subject have been published recently.[1−4] Accordingly, important results regarding the electronic properties, the adsorption behavior, and the catalytic activity of such model catalysts have been obtained. Recently, another type of model catalyst system has been suggested,[5] which consists of a metal single-crystal surface decorated with submonolayer quantities of an oxide phase. In view of the complementary nature to the "real" catalysts, this oxide-on-metal system may be regarded conceptually as an "inverse" or "inverted" model catalyst. Here, the catalytically active phase is the oxide-free surface of the metal substrate and the metal-oxide boundary. The concept of this "inverse model system" offers the possibility to evaluate proximity effects of the metal-oxide interface, that is, to investigate possible differences in the reactivity between adsorption sites in the immediate vicinity of the metal-oxide interface and at a distance away from it.

To establish the optimal conditions for the fabrication of structurally well-defined inverse model catalyst surfaces, the growth and the structure of ultrathin vanadium oxide films on Pd(111) surfaces have been studied systematically over the past few years in our group.[6−10] Vanadium oxides were chosen as the oxide phase because of their importance in practical catalysis. Furthermore, since vanadium oxides occur in various oxidation states, strong metal support interaction (SMSI) effects, which are well documented for supported metal particles,[11] may be expected also for inverse model catalyst geometries. A recent high-temperature scanning tunneling microscopy (STM) investigation[12] has revealed a wetting−dewetting behavior on the vanadium oxide/Pd(111) system as a result of reduction−oxidation cycles, a phenomenon which is analogous to the encapsulation of supported Pt nanoparticles by a thin layer of reduced titanium oxide.[13]

In this investigation, we have employed the vanadium oxide/Pd(111) inverse model catalyst system to study the effects of oxidation and reduction treatments on the structure and reactivity of a heterogeneous oxide-on-metal surface. We have focused on the low oxide coverage regime (below one monolayer), at which structurally well defined oxide-on-metal surfaces can be prepared. The morphology of the vanadium oxide/Pd(111) surfaces has been characterized experimentally by scanning tunneling microscopy (STM), and the surface structures of the oxide layers have been determined theoretically by ab initio density functional theory (DFT). The adsorption of CO at room temperature has been used to probe the adsorption properties of the free Pd sites. Using the ability of high-resolution X-ray photoelectron spectroscopy (HR-XPS) with synchrotron radiation to distinguish between different adsorption sites on metal surfaces, substrate (Pd $3d_{5/2}$) and adsorbate (C 1s) core levels have been monitored here as a function of the oxide coverage and oxidation state. By varying the vanadium oxide coverage, the relative number of adsorption sites affected and unaffected

* Corresponding author. Fax: +43 316 380 9816. E-mail: svetlozar.surnev@uni-graz.at.
† Karl-Franzens Universität Graz.
‡ Universität Wien.
§ Lund University.

10.1021/jp0223408 CCC: $25.00 © 2003 American Chemical Society
Published on Web 04/29/2003

by the oxide phase boundary has been varied. Changes in the oxide film structure and stoichiometry resulting from oxidation−reduction treatments have an influence on the adsorption properties of the metal-oxide interface and, thus, on the catalyst's reactivity.

2. Experiment and Theory

2.1. Experiment. The experiments have been carried out in three different UHV systems with base pressures in all systems below 1×10^{-10} mbar. High-resolution X-ray photoelectron spectroscopy (HR-XPS) measurements were performed at beamline I311 at the Swedish synchrotron radiation facility MAX-Lab in Lund. The beamline and the experimental end station have been described previously.[14] Briefly, I311 at MAX II is an undulator beamline with a modified SX-700 monochromator and an end station equipped with a hemispherical SCIENTA SES 200 spectrometer. Photon energies of 340 and 400 eV were used for exciting electrons from the C 1s and Pd $3d_{5/2}$ core levels, respectively. The corresponding experimental resolution was better than 80 meV ($h\nu = 340$ eV) and 100 meV ($h\nu = 400$ eV). All spectra shown in this paper were measured at normal emission and at room temperature. The binding energy scale was calibrated with respect to the Fermi edge of the crystal in each case. The spectra have been normalized to the secondary electron background at a few electron volts lower binding energy (BE) than the respective core level peak. The C 1s and Pd $3d_{5/2}$ XPS spectra were analyzed by peak decomposition using Donjiac−Ŝunjic line shapes[15] convoluted with Gaussians.

The STM and HREELS measurements were performed in Graz in two different custom-designed UHV systems. One is equipped with a variable temperature STM (Oxford Instruments), as described in more detail elsewhere.[7] The STM images were recorded in a constant current mode at room temperature. Electrochemically etched W tips, cleaned in situ by electron bombardment were used. Tunneling currents as low as 50 pA were employed in order to minimize the influence of the tip on the oxide structures. The other UHV system is equipped with an ErEELS 31 spectrometer for high-resolution electron energy loss spectroscopy (HREELS) measurements. The HREELS spectra were taken at a specular angle of 60° from the surface normal, at an incident beam energy of 5.5 eV and with the crystal at room temperature. The energy resolution was set to ∼5 meV as measured at the full width of half-maximum of the reflected primary electron beam.

In all experimental systems, vanadium oxide/Pd(111) inverse model catalysts have been fabricated under identical conditions, that is, evaporation of V onto the clean Pd(111) surfaces at 250°C in an oxygen atmosphere of 2×10^{-7} mbar. Vanadium (purity 99.8%, Goodfellow Metals) was deposited from a well degassed water-cooled electron beam evaporator (Omicron EFM3). The V deposition rate was monitored by a quartz crystal microbalance and was varied between 0.1 and 0.4 monolayer/min. The vanadium oxide coverages are given in monolayer equivalents (MLE), which corresponds to the evaporated amount of V as determined by the quartz microbalance and referred to the density of Pd(111) surface atoms (1.52×10^{15} atoms cm^{-2}). The vanadium oxide/Pd(111) surfaces have been subjected to two different post-evaporation treatments involving reduction in a hydrogen atmosphere of 2×10^{-7} mbar at 250 °C and reoxidation in an oxygen atmosphere of 2×10^{-7} mbar at 250 °C. We will refer throughout the paper to the resulting surfaces as being in the *reduced* and *oxidized* state, respectively. The latter is indistinguishable from the as-evaporated state.

CO adsorption at room temperature was used to probe the oxide-free Pd sites on the vanadium oxide/Pd(111) surfaces. CO was dosed from the system ambient via a leak valve, and the exposures are given in Langmuir ($1\ \text{L} = 1 \times 10^{-6}$ Torr s). The CO coverage (which is proportional to the free Pd area) was estimated from the intensity of the C 1s core-level peak, using the CO saturation coverage at room temperature of 0.5 monolayer as a calibration point.[16] It is important to mention that CO does not cause a reduction of the oxide films. This is confirmed by the absence of changes in the oxide structure and composition during CO exposure, as monitored by STM and XPS spectra of the V 2p core level and valence band regions. Small reduction effects following CO exposures have been reported in our previous HREELS study.[8] Recently, however, it appeared that the reason for such oxide reduction was the presence of small amounts of hydrogen in the UHV system background.[10]

2.2. DFT Calculations. The first-principles calculations are based on density functional theory (see, e.g., refs 17,18) and employ a plane wave basis set.[19,20] As in previous work (see refs 9,10,21), the Vienna ab initio simulation package (VASP)[22,23] has been used, wherein the most recent version the interaction between the ions and electrons is described by the projector augmented wave (PAW)[24] method in the implementation of Kresse and Joubert.[25] The technical parameters were similar to those used in refs 9,10,21. The Pd surface has been modeled typically by a four-layer Pd slab (two layers have been allowed to relax), and the lattice constant has been fixed to the theoretical Pd fcc lattice constant ($a_{\text{theory}} = 3.95$ Å, $a_{\text{exp}} = 3.89$ Å). The generalized gradient approximations (GGA) of Perdew and Wang,[26,27] commonly referred to as PW91, have been used throughout this work.

To sample the band structure, grids corresponding to 8×8 k-points in the primitive surface cell were chosen. For the (2×2) and (4×4) supercells, this corresponds to 4×4 and 2×2 k-points, respectively. The (4×4) surface was modeled by a three-layer slab. Tests for a few selected (4×4) structures indicated that the formation energies of the considered oxides are accurate to ∼20 meV, even with three-layer slabs. The core level shifts were calculated including final state effects using a modified version of the projector-augmented wave method. In the present PAW core-level implementation, a single core electron is excited from the core to the valence states. Screening by the core electrons is not taken into account (i.e., the other core electrons are kept frozen in the configuration for which the PAW potential was generated). Screening by the valence electrons is included, however. Tests indicating the reliability of this approach by comparison with full potential calculations will be presented elsewhere.[28] Since this approach is relatively new, additional calculations were performed with PAW potentials in which one core electron was moved from the core to the valence during the generation of the potential. The results of these test calculations were practically identical with the reported values. For the determination of the core level shifts, the technical parameters (such as k-points and slab thickness) differ somewhat from the other calculations. Six-layer slabs were used for supercells with a periodicity of (2×2), and the k-point grid was increased to $6 \times 6 \times 1$. For the larger supercells with a (4×4) periodicity, the number of layers was, however, again reduced to three. For the clean surface and the s-V_2O_3 structure, a reduction from six to three layers introduced errors of 20 meV in the core level shift, which, hence, is the estimated error for the core level shifts reported for the (4×4) supercells.

STM images were simulated following loosely Tersoff and Haman.[29] To simulate the constant current STM images, the local energy-resolved density of states $\rho(r, \epsilon_{\text{Fermi}})$ was evaluated,

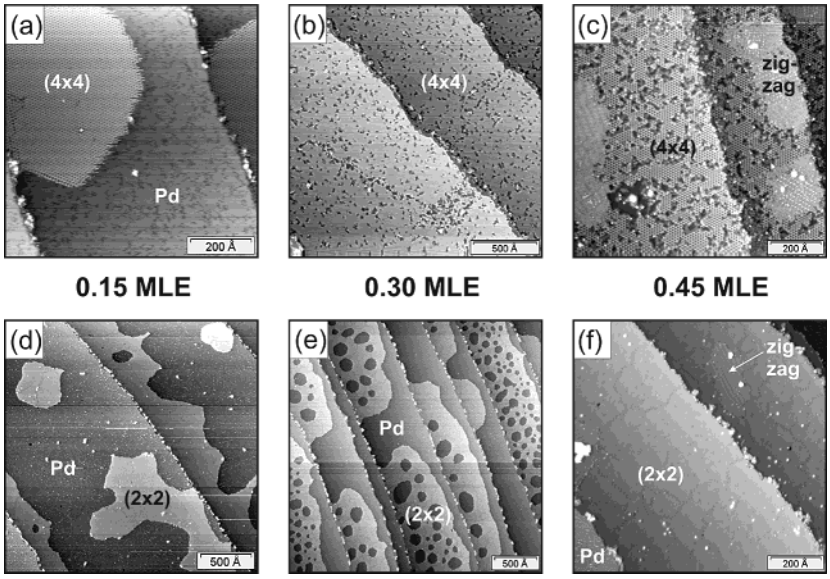

Figure 1. Large-scale STM images of three different vanadium oxide layers on Pd(111) corresponding to coverages of 0.15, 0.30, and 0.45 MLE: (a−c) oxidized state, (d−f) reduced state.

and iso-surfaces of constant charge density $C = \rho(r,\epsilon_{\text{Fermi}})$ were determined. The constant C was chosen so that the core iso-surface distance was always ∼3 Å.

The vibrational spectra of the considered oxide phases were calculated using finite differences. For the (2 × 2) and (4 × 4) superstructures, again four- and three-layer-thick Pd slabs were used, respectively. The substrate was kept frozen in the course of the frozen phonon calculations. Each atom in the oxide was displaced by ±0.02 Å in each direction. From this calculation, the interatomic force constants were determined, and the mass-weighted force constant matrix was diagonalized. This yields the vibrational frequencies and the vibrational eigenmodes of the oxides. The intensities of the loss peaks associated with each mode were estimated by determining the derivative of the dipole with respect to each vibrational mode (the dynamical dipole).

3. Results and Discussion

Within the concept of the inverse model catalyst, surfaces have been prepared on which vanadium oxide and Pd areas of different size coexist. Three submonolayer oxide coverages of 0.15, 0.30, and 0.45 MLE were chosen for this purpose. In Section 3.1, the morphology and structure of the resulting vanadium oxide/Pd(111) surfaces in the oxidized and the reduced state will be presented. The effects of the reduction−oxidation treatments and the oxide coverage on the reactivity of the vanadium oxide/Pd(111) surfaces will be described in Section 3.2.

Structure. Figure 1 shows the typical morphology of vanadium oxide/Pd(111) surfaces subjected to oxidation (Figure 1a−c) and reduction (Figure 1d−f) treatments. In the oxidized state, the vanadium oxide/Pd(111) surface with 0.15 MLE oxide coverage (Figure 1a) consists of well ordered oxide islands with a (4 × 4) periodicity and oxide-free areas on the Pd terraces. At a critical coverage of ∼0.30 MLE, the (4 × 4) oxide phase almost completely covers the Pd(111) substrate, with the exception of numerous but small defect areas (Figure 1b). The atomic resolution STM image of the (4 × 4) oxide phase is presented in Figure 2a along with a V_5O_{14} structure model (Figure 2b). This model was determined by a search of the configuration space using DFT calculations. In the course of these calculations, ∼20 different trial models were constructed applying chemical intuition and extensive simulated annealing

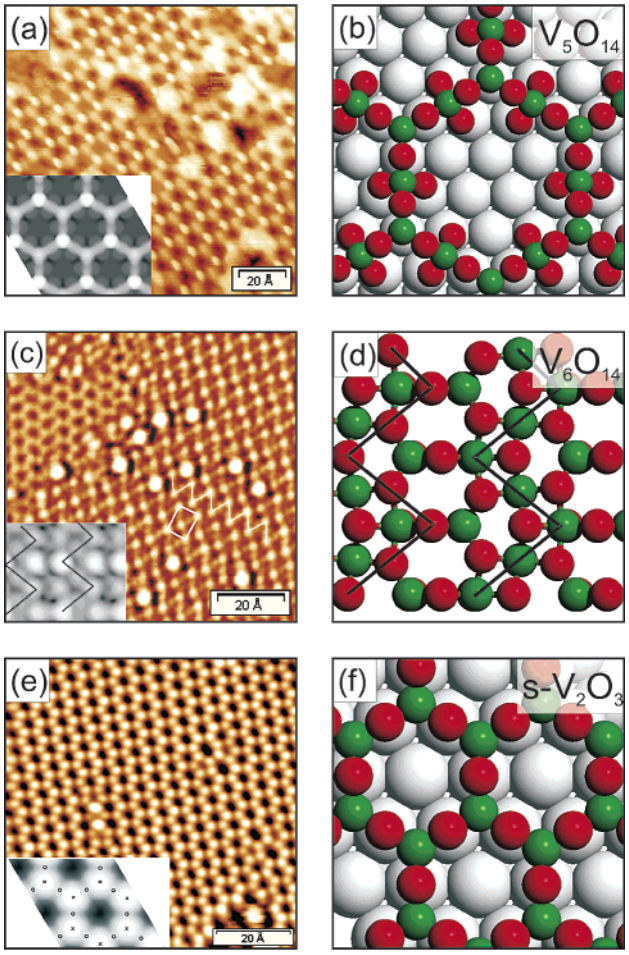

Figure 2. Atomically resolved STM images (left panels) and DFT models (right panels) of the (4 × 4)-V_5O_{14} (a−b), zigzag-V_6O_{14} (c−d), and (2 × 2)-surface-V_2O_3 (e−f) oxide phases. The insets in a−c display the STM simulations for the respective models.

simulations. The V coverage (∼0.3−0.45 monolayer of V) and the stoichiometry (close to V_2O_5) were restricted to lie in the range estimated from experiments. When the phase diagram of V_xO_y on Pd was extended to include the new models (see ref 21), only the V_5O_{14} structure was shown to be stable. This

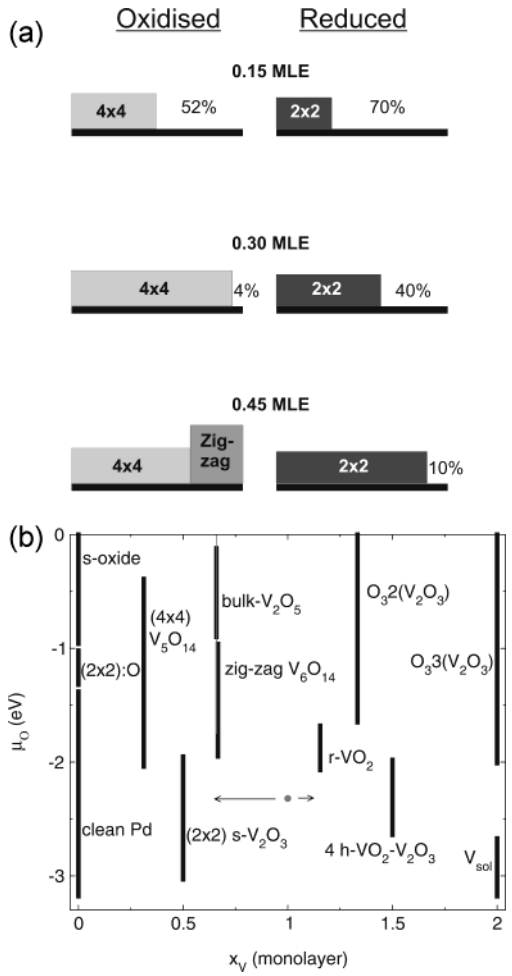

Figure 3. (a) Schematic drawing of the vanadium oxide/Pd(111) surface, giving the distribution of the free Pd area (in %) as a function of the oxide coverage for the oxidized and reduced surfaces. (b) Surface phase diagram as a function of the oxygen pressure μ_O and the vanadium coverage x_V. Stable phases are indicated with black bars. The chemical potential μ_O can be related to the partial pressure of oxygen and the temperature, T, through $\mu_O(T, p) = \mu_O(T, p^0) + 1/2\ k_BT\ \ln(p/p^0)$. Typical preparation conditions of 2×10^{-7} mbar and 250 °C correspond to roughly $\mu_O = -0.9$ eV.[35] When the surface is prepared at $x_V = 1$ and $\mu_O = -0.9$ eV (●), two oxides should form, as indicated by the arrows.

particular model was determined by simulated annealing. The V_5O_{14} layer is oxygen-terminated at both the metal and the vacuum interface and contains V atoms in unusual tetrahedral O coordination. The structure is quite open, leaving a relatively large number of Pd atoms uncovered (six per (4 × 4) unit cell). The inset of Figure 2a shows an STM simulation, based on the V_5O_{14} model, which agrees well with the experimental STM image. The (4 × 4) monolayer coverage, that is, the V coverage at which the (4 × 4)-V_5O_{14} layer fully covers the Pd(111) surface, is 0.3125 MLE (5 V per 16 Pd atoms), which is consistent with the STM image observed at 0.30 MLE (Figure 1b).

At 0.45 MLE (Figure 1c), the (4 × 4) structure is partially replaced by a denser oxide phase with the so-called "zigzag" structure.[10] The latter consists of zigzag stripes, clearly seen in the atomically resolved STM image of Figure 2c, which are running along equivalent Pd <1$\bar{1}$0> directions and are separated by a distance of 8.7 Å. The zigzag structure is not commensurate with the Pd(111) substrate and has a rectangular unit cell with dimensions of 6.9 × 8.7 Å^2. The DFT calculations suggest that the zigzag vanadium oxide can be rationalized in terms of a

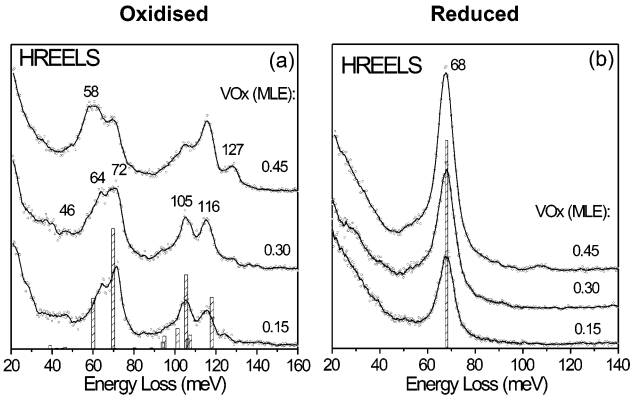

Figure 4. HREELS phonon spectra recorded in specular scattering geometry of 0.15, 0.30, and 0.45 MLE vanadium oxide layers in the oxidized (a) and reduced (b) states. The bars indicate the calculated dipole active phonon spectra for the V_5O_{14} (a) and s-V_2O_3 (b) oxide structures.

model with a formal V_6O_{14} stoichiometry, displayed in Figure 2d. The corresponding STM simulation image is shown in the inset of Figure 2c and is in good agreement with the experimental one. The zigzag-V_6O_{14} layer is also O-terminated at both interfaces, but in contrast to the (4 × 4) phase, it is more dense and leaves no Pd surface atoms uncovered.

The vanadium oxide/Pd(111) surfaces in the reduced state (Figure 1d−f) show two-dimensional oxide islands with a (2 × 2) periodicity, which increase in area with the oxide coverage. At a critical coverage of ∼0.5 MLE,the Pd(111) surface becomes completely covered by the (2 × 2) oxide phase. The atomically resolved STM image (Figure 2e) shows bright maxima, arranged in a (2 × 2) honeycomb lattice, and recent DFT calculations have revealed an interface-stabilized vanadium oxide phase with a formal V_2O_3 stoichiometry (the phase has been called surface- or s-V_2O_3, Figure 2f).[7,21] The monolayer coverage of the s-V_2O_3 phase is 0.5 MLE (2 V per four Pd atoms), which is consistent with the STM image in Figure 1f, where almost the entire Pd(111) surface is covered by the (2 × 2) layer at 0.45 MLE. Some remainders of the zigzag phase, which cannot be reduced under the employed conditions, are still visible here as minority species. Note that in contrast to the (4 × 4) and zigzag structures, the s-V_2O_3 layer is V-terminated at the metal−oxide interface and that 1 Pd atom per (2 × 2) unit cell remains uncovered.

The composition and distribution of the vanadium oxide phases and the free Pd(111) areas as a function of the oxide coverage and the oxidation−reduction treatment are summarized schematically in Figure 3a. For each oxide coverage, the relative area of the oxide-free Pd parts of the surface has been evaluated from the monolayer coverages of the (2 × 2) and (4 × 4) phases. Figure 3b indicates the stable phases as a function of the oxygen pressure, μ_O, and as a function of the vanadium coverage, x_V, as determined by the ab initio calculations. Details on the construction of this phase diagram were given in ref 21. Compared to the previous calculations, additional models in the low coverage regime were considered; above 1 monolayer, the results are, however, identical to those presented in ref 21. Clearly, the (4 × 4) structure is energetically favorable under O-rich conditions, and the zigzag phase dominates the phase diagram at intermediate V coverage and oxygen pressure.

Figure 4 shows HREELS spectra of the phonon region of the vanadium oxide/Pd(111) surfaces discussed above in the oxidized (Figure 4a) and the reduced state (Figure 4b). For ∼0.3 MLE or less, the HREELS spectra from the oxidized films contain phonon losses at 46, 64,72, 105, and 116 meV. These

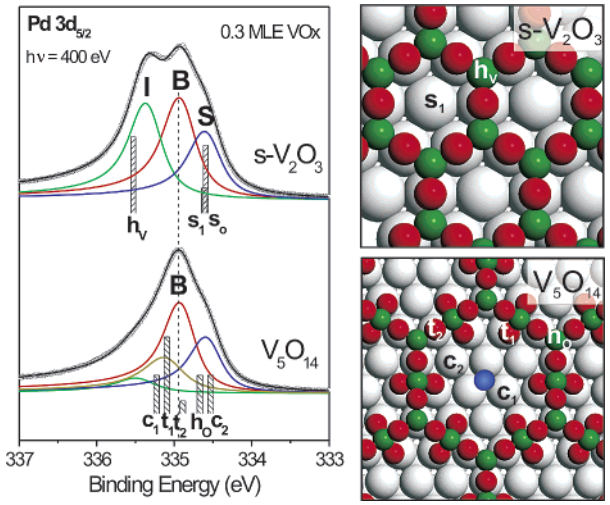

Figure 5. Pd $3d_{5/2}$ core level photoemission spectra of 0.30 MLE vanadium oxide/Pd(111) surfaces in the reduced (top) and oxidized (bottom) state. The bars display the calculated surface core level components for the various Pd sites at the s-V_2O_3/Pd(111) and V_5O_{14}/Pd(111) interfaces, as indicated in the corresponding models on the right-hand side. One oxygen atom (blue circle) occupies the fcc hollow site in the center of the Pd atoms within the pockets of the V_5O_{14} structure.

can be associated with the (4 × 4)-V_5O_{14} structure, which is the only oxide phase in this coverage range (Figure 1a,b). The experimental loss peaks are consistent with the dipole active phonon frequencies and intensities as calculated from the V_5O_{14} model (displayed as bars in Figure 4a). At 0.45 MLE, the additional peaks at ~58 and 127 meV in the loss spectrum may be related to the zigzag V_6O_{14} structure (see Figure 1c). The HREELS spectra of the reduced vanadium oxide films (Figure 4b) are all characterized by the presence of a single loss peak at 68 meV, which is due to the calculated Γ-point dipole active optical phonon mode of the (2 × 2) s-V_2O_3 structure.[7]

The substrate Pd $3d_{5/2}$ core level spectra reveal further details about the structure of the vanadium oxide/Pd(111) interface. In Figure 5, Pd $3d_{5/2}$ core level spectra taken from 0.3 MLE vanadium oxide/Pd(111) surfaces in the reduced (top) and oxidized (bottom) states are compared. The clean Pd $3d_{5/2}$ spectrum (not shown) consists of two components with a binding energy (BE) of 334.90 and 334.62 eV, which are due to photoemission from bulk and surface Pd atoms, respectively. The clean surface component exhibits a surface core level shift (SCLS) to lower BE of −280 meV relative to the bulk component in agreement with previous observations.[30] The present theoretical calculations predict a surface core level shift of −304 meV for the clean Pd(111) surface, in good agreement with experiment. For the reduced 0.3 MLE vanadium oxide (s-V_2O_3) layer, the Pd $3d_{5/2}$ spectrum shows a well resolved maximum at the high BE side due to the appearance of a so-called interface component, labeled *I*, which is related to the Pd surface atoms capped by the s-V_2O_3 layer. This *I* component exhibits a SCLS of +450 meV, which is specific for the s-V_2O_3/Pd(111) interface. The interface consists of V atoms occupying fcc and hcp hollow Pd(111) sites[7] (labeled h_V on the s-V_2O_3 model at the right-hand side of Figure 5). The theory predicts a positive SCLS of +620 meV due to the coordination to V atoms, somewhat larger than the experimental one (see Table 1 and the bar h_V under the s-V_2O_3 spectrum of Figure 5). The middle component (marked B) appears at a BE of 334.90 eV and is, therefore, associated with photoemission from the Pd bulk atoms. The component at the low BE side (marked S) exhibits a SCLS of −330 meV, which is very close to the SCLS

TABLE 1: Calculated and Experimental Pd $3d_{5/2}$ Surface Core Level Shifts (SCLSs) in meV for the (2 × 2)-s-V_2O_3 Structure[a]

	site	
	s_1	h_V
theory	−290 (1)	+628 (3)
experiment	−330 (s_1 + s_o)	+450

[a] The occupancy of the site per (2 × 2) unit cell is given in parentheses.

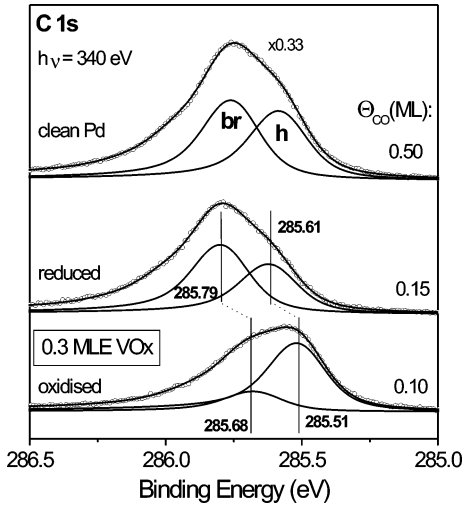

Figure 6. C 1s core level photoemission spectra of the room-temperature CO saturated clean Pd(111) surface (top) and of 0.30 MLE vanadium oxide/Pd(111) surfaces in the reduced (middle) and oxidized (bottom) state. The CO coverage (in mol), as determined from the integrated intensity of the C 1s peaks, is given on the right-hand side of the figure.

of the clean Pd(111) surface. Two kinds of surface Pd atoms contribute to this intensity. At 0.3 MLE, ~40% of the Pd(111) surface remains oxide-free (see Figures 1 and 3), and will contribute emission at the same binding energy as for the clean surface (bar s_o under the s-V_2O_3 spectrum of Figure 5). The second contribution comes from the central Pd atom within the (2 × 2) oxide unit cell, which is not coordinated to V atoms (marked s_1 on the s-V_2O_3 model). For these atoms, theory predicts a core level shift of −290 meV, also very close to that for the clean Pd(111) surface. As will be shown below (Figure 8), the spectral weights of the h_V and s_1 peaks scale up with increasing s-V_2O_3 coverage, while that of s_o progressively decreases, vanishing at the (2 × 2) monolayer coverage of 0.5 MLE.

The (4 × 4)-V_5O_{14}/Pd(111) interface is much more complex (see V_5O_{14} model), which results in a completely different Pd $3d_{5/2}$ line shape (Figure 5, bottom spectrum). The V_5O_{14} layer is O-terminated at the oxide/Pd interface with eight O atoms per unit cell occupying three different Pd surface sites: six near on top (t_1), 1 on top (t_2) and 1 hollow (h_O). The latter O atom is not visible on the V_5O_{14} structure model, since it is capped by a V atom. Within the pockets of the (4 × 4) unit cell, there are six Pd atoms, three central (c_1) and three corner (c_2), which are not coordinated to the oxide O atoms. Hence, at least five different interface components have to be included in the decomposition analysis of the Pd $3d_{5/2}$ core-level spectrum. Unfortunately, the latter exhibits a quite structureless shape, which makes the decomposition analysis not very reliable. Nevertheless, a relatively good fit could be obtained with four core-level components (with binding energies of 334.56, 334.90, 335.10, and 335.44 eV), with shape parameters equal to those

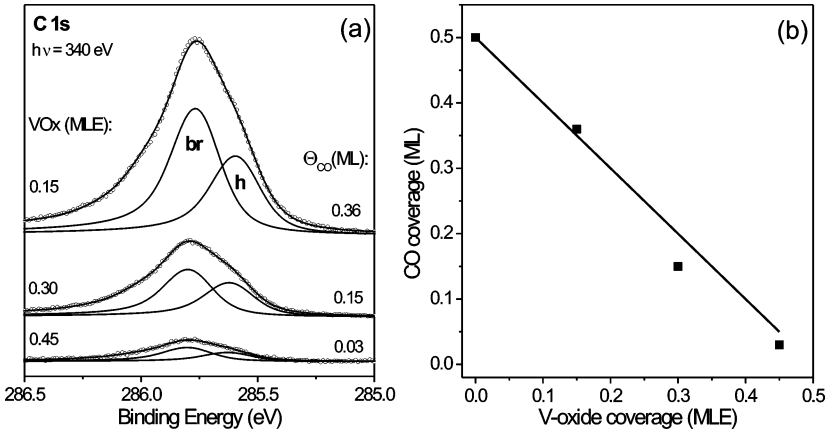

Figure 7. (a) C 1s core level photoemission spectra of reduced vanadium oxide/Pd(111) surfaces for different oxide coverages. (b) Plot of the CO coverage (■), as determined from the integrated intensity of the C 1s peaks of Figure 6a, versus the vanadium oxide coverage (MLE). The solid line represents the calculated oxide coverage dependence of the CO coverage, as determined from simple geometry considerations (see text).

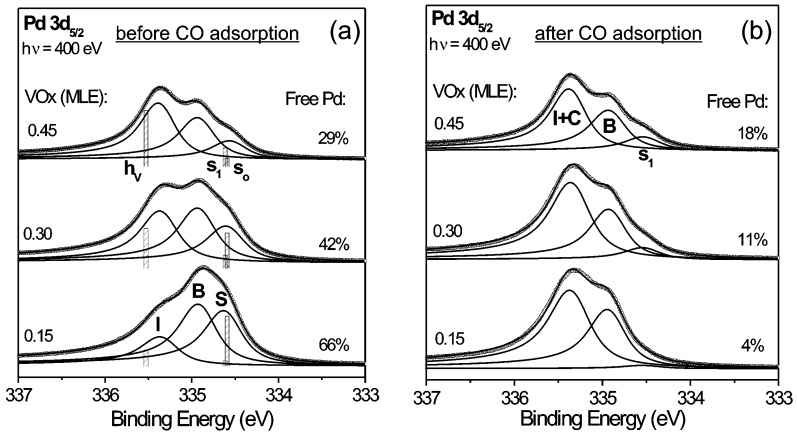

Figure 8. Pd $3d_{5/2}$ core level photoemission spectra of various vanadium oxide/Pd(111) surfaces in the reduced state taken (a) before, and (b) after a saturation dose of CO at room temperature. The bars in (a) indicate the calculated core level components.

used for fitting the s-V_2O_3 Pd $3d_{5/2}$ spectrum. The peak with a BE of 334.9 eV can again be related to the bulk (*B*) core level component. The theory has considered two cases: (i) V_5O_{14}/Pd(111) surface with all Pd atoms uncovered within the pockets and (ii) with one oxygen atom adsorbed in the fcc hollow site formed by the central Pd atoms (c_1). The second case accounts for the possibility of oxygen adsorption on the Pd(111) surface, which shifts the c_1 component from the low BE side (near degenerate with c_2) to the high BE side. The DFT calculations indicate that one oxygen atom adsorbed at the fcc Pd hollow site in the pockets of the (4 × 4) oxide structure is favorable. The adsorption energy with respect to molecular oxygen is 1.30 eV, and this is almost identical to the adsorption energy of oxygen on the clean Pd(111) surface (1.36 eV in our calculations). One should have in mind that this adsorbed oxygen atom is not a part of the (4 × 4)-V_5O_{14}/Pd(111) structure and is, therefore, not shown on the DFT model in Figure 2b.

The calculated Pd $3d_{5/2}$ SCLSs for the (4 × 4) V_5O_{14}/Pd-(111) surface (with and without additional oxygen atom) are listed in Table 2. It is readily seen that the calculated SCLSs for the V_5O_{14}/Pd(111) surface with bare pockets do not account for the presence of a significant spectral intensity at the higher BE side of the bulk component. A better agreement with the experiment is found for the case in which the chemisorbed O in the pockets induces a positive SCLS of 328 meV. The latter value is very close to the experimentally observed SCLS of 380 meV for the (2 × 2)O−Pd(111) surface, where O atoms are known to occupy fcc Pd sites, also.[31] The calculated core level peaks (displayed as bars) reproduce the experimental V_5O_{14} Pd $3d_{5/2}$ XPS spectrum in Figure 5 qualitatively. Note that at 0.3 MLE, the portion of the free Pd area not covered by the (4 × 4) oxide overlayer is only ∼4% and can be neglected in the determination of the spectral weight of the calculated peaks.

TABLE 2: Calculated Pd $3d_{5/2}$ Surface Core Level Shifts (SCLS) in MeV for the (4 × 4)-V_5O_{14} Structure with and without One O Atom Chemisorbed in the Center, as Compared to the Experimentally Determined Peak Components[a]

	site				
	c_1	c_2	h_O	t_1	t_2
V_5O_{14}	−297 (3)	−378 (3)	−282 (3)	+76 (6)	−77 (1)
V_5O_{14} + O	+328 (3)	−370 (3)	−231 (3)	+194 (6)	−10 (1)
experiment	+540	−340	+200		

[a] The occupancy of the site per (4 × 4) unit cell is given in parentheses.

Adsorption of CO. Adsorption of CO at room temperature has been used to test the reactivity of the various vanadium oxide/Pd(111) surfaces. Since CO does not adsorb onto the vanadium oxide surface at room temperature,[5] the adsorption of CO allows one to follow the influence of the morphology and the structure of the oxide phase on the surface chemistry of the Pd sites.

Before investigating the CO adsorption properties as a function of the oxide coverage, it is useful to discuss the effects of the reduction−oxidation treatment at a fixed oxide coverage. Figure 6 shows C 1s core level spectra taken after exposing the clean (top spectrum) and 0.3 MLE vanadium oxide-covered Pd-

(111) surfaces in the reduced (middle spectrum) and oxidized (bottom spectrum) states to a saturation dose (~5 L) of CO at room temperature. The corresponding CO coverages, determined from the C 1s integrated intensity and normalized to the value of 0.5 monolayer for the clean Pd surface, are displayed on the right-hand side of Figure 6. For CO adsorption onto the clean Pd(111) surface, the C 1s peak consists of two components with binding energies of 285.54 eV (*h*) and 285.74 eV (br), which are due to adsorption of CO molecules in 3-fold hollow and bridge sites, respectively, as established previously.[16] The theoretically predicted BE difference between the br and *h* components is 190 meV, in excellent agreement with the experiment. Each of these components is coupled to vibrational satellites, which have binding energies shifted by 200 and 400 meV (not shown here for reasons of clarity) as a result of the excitation of intramolecular stretching vibrations of adsorbed CO in the photoemission process.[16] For CO adsorption onto the 0.3 MLE vanadium oxide/Pd surfaces, the C 1s peak shape can also be decomposed into two components (*h* and br) with vibrational fine structure. The shape of the C 1s spectrum from the reduced catalyst surface is similar to that of the clean Pd surface. Only a rigid shift of ~0.06 eV to higher BE is detected for the *h* and br components. The *h*/br ratio is not significantly altered, suggesting that the CO molecules occupy the same adsorption sites as on the clean Pd(111) surface. In contrast, on the oxidized surface, the 3-fold hollow sites become preferably populated, as evident from the increased intensity of the *h* component. The peak positions of the *h* and br components are now shifted by ~0.1 eV to lower binding energies, which is due to the altered electronic structure of the oxidized 0.3 MLE vanadium oxide/Pd surface. Note that the experimentally determined saturation CO coverage on the latter surface (0.1 monolayer) is much larger than the CO coverage of 0.02 monolayer, which is expected from the model in Figure 3, assuming that CO only adsorbs onto the oxide-free Pd areas ($0.5 \times 0.04 = 0.02$ monolayer). As explained below, the reason for this discrepancy is that CO molecules adsorb into the pockets of the (4×4) oxide layer, thereby replacing the chemisorbed O atoms.

Next, we examine the effect of the oxide coverage on the adsorption behavior of CO and consider first the reduced vanadium oxide/Pd(111) surfaces. Figure 7a displays C 1s photoemission spectra after a saturation dose of ~5 L of CO at room temperature on reduced surfaces with varying vanadium oxide coverage. The resulting CO coverage is indicated on the right-hand side of Figure 7a. The decomposition analysis reveals that the C 1s spectra exhibit similar line shapes for the various oxide coverages, which are determined by the adsorption of CO molecules in a mixture of hollow and bridge sites on the free Pd(111) surface areas. Similar results have been obtained for CO thermal desorption spectra from a s-V_2O_3/Pd(111) surface, which exhibit a shape identical to that of CO desorption from clean Pd(111).[32] This indicates that the CO adsorption is not modified by the presence of the s-V_2O_3 phase (apart from the progressive blocking of CO sites by the oxide), even when the latter covers more than 90% (at ~0.45 MLE) of the Pd (111) substrate. This behavior is also illustrated in Figure 7b, where the experimentally determined CO coverage (squares) has been plotted as a function of the vanadium oxide coverage. The experimental data follow very closely the line from the CO saturation coverage on clean Pd(111) to the point of complete s-V_2O_3-covered Pd surface (0.5 MLE) where no CO adsorbs.

Figure 8 shows corresponding Pd $3d_{5/2}$ core level spectra from the reduced vanadium oxide/Pd(111) surfaces taken before (Figure 8a) and after (Figure 8b) CO saturation adsorption. Prior to the CO adsorption, the increase of the s-V_2O_3 coverage results in a progressive increase of the intensity of the interface component I, at the expense of the free Pd component *S*. Remember that the latter is calculated to consist of two nondegenerate components s_o and s_1, related to the oxide-free Pd areas and the central Pd atoms within the (2×2) oxide unit cell, respectively. Obviously, at low s-V_2O_3 coverages the s_o peak dominates the *S* component, while close to the s-V_2O_3 monolayer coverage (0.5 MLE), the s_1 becomes dominant. On the right-hand-side of Figure 8a, the free Pd surface fraction for each vanadium oxide coverage is given, as estimated from the intensity ratio $S/(S + I)$. At 0.45 MLE, there is still a clearly detectable contribution of the *S* component in the Pd $3d_{5/2}$ peak intensity, which corresponds to ~29% free Pd sites. This value agrees quite well with the free Pd surface fraction of 32.5%, as estimated from simple geometrical considerations for 0.45 MLE (10% in s_o and 22.5% in s_1). A small shift of the *S* component to lower binding energies is observed with increasing the s-V_2O_3 coverage, consistent with their change in weight, as discussed below.

The CO adsorption at room temperature leads to the appearance of an additional CO induced Pd component *C* (Figure 8b), which is site-specific. Two such components with binding energies of ~335.2 and 335.4 eV due to the population of hollow and bridge sites, respectively, have been detected in fitting the Pd $3d_{5/2}$ peaks for the CO adsorption on clean Pd(111) in our previous study.[16] Unfortunately, these values are very close to the binding energy of the interface component of the s-V_2O_3/Pd(111) surface (~335.35 eV), which makes the decomposition analysis for the high-binding energy part of the Pd 3d structure problematic. To overcome this problem, the Pd 3d spectra after the CO adsorption have been fitted by a single, but broader spectral component, labeled $I + C$, which accounts for the combined effect of the interface and CO-induced components while keeping the shape parameters of the *B* and *S* components unchanged. Since the CO adsorption on the s-V_2O_3/Pd(111) surface takes place only on the oxide-free Pd(111) areas, it is expected that the *C* component should grow in intensity at the exclusive expense of the oxide-free Pd surface component s_o. This gives us the opportunity to unambiguously resolve the contribution of the central Pd atoms (s_1) within the (2×2) oxide layer in the *S* component of the Pd $3d_{5/2}$ core level spectrum. These Pd atoms are inaccessible to CO adsorption at room temperature, as predicted by the DFT calculations, which showed a large barrier of 400 meV for the CO adsorption on the (2×2) oxide structure.[7] Nevertheless, they contribute to the Pd $3d_{5/2}$ core level spectrum. Their spectral weight should increase for higher s-V_2O_3 coverage, as is, indeed, experimentally observed (Figure 8b).

The oxide coverage dependence of the free Pd area, as determined from the weight of the *S* component of the Pd $3d_{5/2}$ spectra, before (circles) and after (squares) the CO adsorption on the reduced vanadium oxide/Pd surface is displayed in Figure 9a. The solid lines represent the calculated free Pd areas before and after the CO adsorption, by taking into account also the free Pd surface atoms in the interior of the s-V_2O_3 layer. At the limiting oxide coverage of 0.5 MLE, both sets of experimental data approach the value of 25%, in agreement with one uncoordinated Pd atom per (2×2) unit cell. Figure 9b shows the measured core level shift of the surface component *S* (SCLS) as a function the oxide coverage. Before CO adsorption, the SCLS data (circles) show a linear decrease with increasing oxide coverage, starting at the value of −0.28 eV for the clean Pd-

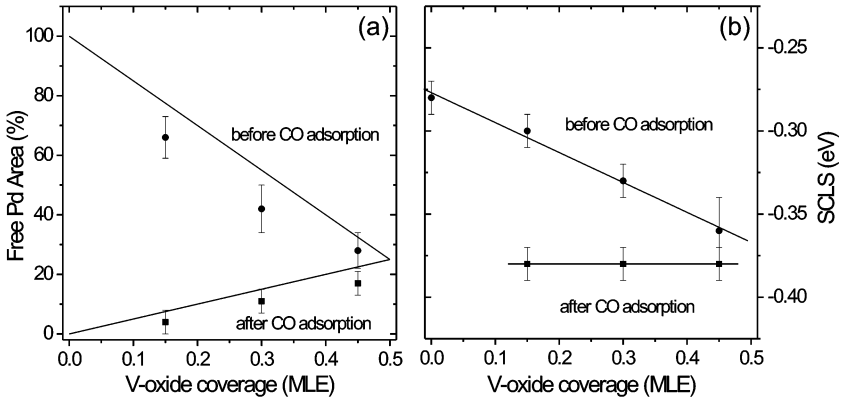

Figure 9. Plot of the free Pd area (a) and of the surface core level shift (SCLS) of free Pd atoms (b) before (●) and after (■) CO adsorption as a function of the vanadium oxide coverage. The SCLSs have been determined from the Pd $3d_{5/2}$ core level spectra of Figure 8. The solid lines in part (a) indicate the calculated oxide coverage dependence of the free Pd area; the solid lines in part (b) are guides to the eye.

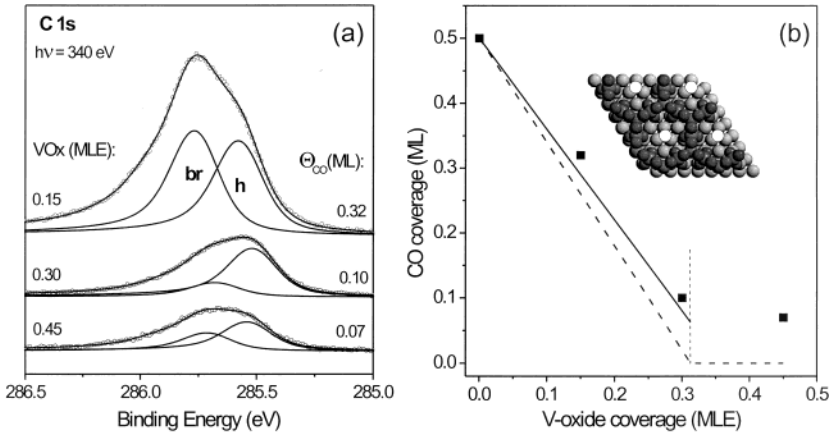

Figure 10. (a) C 1s core level photoemission spectra of oxidized vanadium oxide/Pd(111) surfaces for different oxide coverages. (b) Plot of the CO coverage (■), as determined from the integrated intensity of the C 1s peaks of part (a), versus the vanadium oxide coverage (MLE). The dashed line has been calculated under the assumption that CO adsorbs only on the oxide-free Pd areas. The solid line has been calculated by taking also the CO adsorption within the (4 × 4) layer into account. The inset shows the (4 × 4) structure model with one CO molecule (○) adsorbed in each adsorption pocket.

(111) surface and reaching −0.37 eV at 0.45 MLE. The latter is very close to the SCLS value of −0.38 eV, measured after the CO titration (Figure 8b), which is, therefore, considered as characteristic of the uncovered Pd atoms within the s-V_2O_3 unit cells.

Next, we examine the C 1s spectra of CO adsorbed on the oxidized vanadium oxide/Pd(111) surfaces (Figure 10a). Significant changes in the XPS line shape are observed, as compared to the respective data from the reduced surfaces (Figure 7a), which reflect a different site distribution of the adsorbed CO species. At 0.15 MLE, a small increase in the intensity of the *h* component relative to the br component is visible, while at 0.30 and 0.45 MLE, the hollow component becomes dominant, as a result of a preferential adsorption of CO in hollow sites on the oxidized surfaces. If we assume that CO molecules adsorb only on the oxide-free Pd areas, it remains unexplainable that relatively large amounts of CO are detected on the 0.30 and 0.45 MLE oxide-covered Pd surfaces. As mentioned previously, adsorption on the oxide-free Pd areas can count for only up to 0.02 monolayer of CO at 0.30 MLE, while 0.10 monolayer is experimentally observed. At 0.45 MLE, the entire Pd surface is covered by the (4 × 4), and the zigzag oxide phases (see Figure 1c) and no CO adsorption should take place at room temperature. However, ∼0.07 monolayer of CO is detected on this surface. Figure 10b is a plot of the CO coverage as a function of the vanadium oxide coverage. The experimental data (squares) deviate clearly from the dashed line, which is calculated by assuming CO adsorption on the oxide-free Pd areas only (the latter become 0 at the (4 × 4) monolayer oxide coverage of 0.3125 MLE (dotted line in Figure 10b)). This unexpected CO adsorption behavior can be rationalized if the specific atomic structure of the (4 × 4) V_5O_{14} phase (Figure 2b) is taken into account, where six Pd atoms per (4 × 4) unit cell are left uncovered and may serve as adsorption sites within the (4 × 4) oxide layer. To account for the observed preferential population of hollow sites, we speculate that one CO molecule adsorbs in the middle fcc hollow position of these adsorption pockets (replacing the chemisorbed O atom, which is reacted away as CO_2), as indicated in the inset of Figure 10b. The solid line in Figure 10b, which has been calculated by taking into account the above considerations, is consistent with the experimental data in the oxide coverage range 0−0.3125 MLE. Beyond this range, the (4 × 4) phase partly converts into the zigzag structure, a process that depends on kinetic factors, and the zigzag oxide coverage is not accurately known; thus, it cannot be included in the CO coverage calculations.

The DFT calculations confirm the experimental findings in that CO adsorption is exothermal in the pockets of the (4 × 4) oxide layer. The adsorption energy is very similar to that for CO adsorption on the clean surface, and no adsorption barrier is encountered. The calculations also show that the energy difference between bridge and hollow adsorption sites for CO in the pockets is 80 meV larger than on the clean Pd(111) surface. This will shift the balance in favor of preferential

population of hollow sites in the pockets, in agreement with the experimental observation (see Figure 6).

Recent TDS data of CO adsorption on (4 × 4) oxide-covered Pd(111) surfaces[33] have shown the development of a new CO desorption state at a peak desorption temperature of ~373 K, which is ~100 K lower than the peak desorption temperature of CO on Pd(111). The intensity of this new desorption state was found to scale with the (4 × 4) oxide coverage and may, thus, be associated with the desorption of CO molecules from the (4 × 4) adsorption pockets.

An increasing population of hollow sites by adsorbed CO molecules has also been observed as a function of increasing coverage of vanadium oxide on Pd(111) in our previous studies.[5,8] There, preferential occupation of high-coordination sites of CO in the vicinity of the oxide-metal phase boundary has been proposed.[8] In light of the present results, this interpretation is still essentially correct, although in this earlier investigation, detailed structure information on the oxide films and sufficiently high spectroscopic energy resolution were lacking. Here, we have identified in more detail the adsorption sites in terms of "adsorption pockets" within the (4 × 4) overlayer, and this may prove useful in understanding the chemisorption behavior of more complex probe molecules, for example, C_2H_4,[34] on the oxidized vanadium oxide/Pd(111) inverse model catalyst surfaces.

Summary

The structure of reduced and oxidized vanadium oxide/Pd-(111) inverse model catalyst surfaces has been investigated by STM and ab initio DFT calculations, and the titration of the metal sites on these surfaces by CO has been monitored by core level photoelectron spectroscopy using synchrotron radiation. The STM measurements reveal that vanadium oxide films with well-defined structure and morphology can be prepared by both oxidizing and reducing treatments of the oxide in the coverage range up to 0.5 MLE. The detailed atomic structure of the various vanadium oxide phases has been revealed with the help of DFT calculations. On the reduced vanadium oxide/Pd(111) surfaces, an interface-specific (2 × 2) s-V_2O_3 phase is present, which covers the Pd(111) surface completely at ~0.5 MLE. The XPS results show that on the s-V_2O_3-decorated Pd(111) surfaces, CO adsorbs in a mixture of 3-fold hollow and bridge sites, as on the clean Pd(111) at room temperature. No additional components in the C 1s core level peak have been observed that could be associated with a new state of CO adsorption, for example, molecules at the vanadium oxide/Pd phase boundary. However, a new type of surface Pd sites has been detected in the Pd $3d_{5/2}$ XPS spectra as a result of the specific atomic structure of the s-V_2O_3 layer; these sites, however, are not accessible for the adsorption of CO at room temperature.

The oxidized vanadium oxide/Pd(111) surfaces consist mainly of oxide islands of a (4 × 4)-V_5O_{14} phase, which forms a complete layer at an oxide coverage of ~0.3 MLE. The calculated Pd core level shifts indicate that one oxygen atom is chemisorbed in the holes of this open (4 × 4) structure, which consist of six free Pd atoms ("adsorption pockets"). The C 1s photoemission spectra indicate that the balance of hollow and bridge CO adsorption sites is shifted in favor of the preferential population of hollow sites on the oxidized vanadium oxide/Pd-(111) surface. The latter sites are interpreted in terms of a new type of CO adsorption sites within the adsorption pockets of the V_5O_{14}/Pd(111) surface.

Acknowledgment. This work has been supported by the Austrian Science Foundation (Joint Research Program "Gas Surface Interactions") and by the EU-TMR Program under contract ERB FMGE CT98 0124. J.N.A. acknowledges financial support by the Swedish Natural Science Research Council. The support of the MAX-Lab staff is gratefully acknowledged.

References and Notes

(1) Campbell, C. T. *Surf. Sci. Rep.* **1997**, *27*, 1.
(2) Gunter, P.; Niemantsverdriet; J.; Ribeiro, F.; Somorjai, G. A. *Catal. Rev.-Sci. Eng.* **1997**, *39*, 77.
(3) Henry, C. R. *Surf. Sci. Rep.* **1999**, *31*, 235.
(4) Bäumer, M.; Freund, H.-J. *Prog. Surf. Sci.* **1999**, *61*, 127.
(5) Leisenberger, F. P.; Surnev, S.; Koller, G.; Ramsey, M. G.; Netzer, F. P. *Surf. Sci.* **2000**, *444*, 211.
(6) Leisenberger, F. P.; Surnev, S.; Vitali, L.; Ramsey, M. G.; Netzer, F. P. *J. Vac. Sci. Technol. A* **1999**, *17*, 1743.
(7) Surnev, S.; Vitali, L.; Ramsey, M. G.; Netzer, F. P.; Kresse, G.; Hafner, J. *Phys. Rev. B* **2000**, *61*, 13945.
(8) Sock, M.; Surnev, S.; Ramsey, M. G.; Netzer, F. P. *Top. Catal.* **2001**, *14*, 15.
(9) Surnev, S.; Kresse, G.; Ramsey, M. G.; Netzer, F. P. *Phys. Rev. Lett.* **2001**, *87*, 086102.
(10) Surnev, S.; Kresse, G.; Sock, M.; Ramsey, M. G.; Netzer, F. P. *Surf. Sci.* **2001**, *495*, 91.
(11) Tauster, S. J. *Acc. Chem. Res.* **1987**, *20*, 389.
(12) Surnev, S.; Schoiswohl, J.; Kresse, G.; Ramsey, M. G.; Netzer, F. P. *Phys. Rev. Lett.* **2002**, *89*, 246107.
(13) Dulub, O.; Hebenstreit, W.; Diebold, U. *Phys. Rev. Lett.* **2000**, *84*, 3646.
(14) Nyholm, R.; Andersen, J. N.; Johansson, U.; Jensen, B. N.; Lindau, I. *Nucl. Instr. Methods Phys. Res. A* **2001**, *467−468*, 520.
(15) Donijac, S.; Šunjic, M. *J. Phys. C* **1970**, *3*, 285.
(16) Surnev, S.; Sock, M.; Ramsey, M. G.; Netzer, F. P.; Wiklund, M.; Borg, M.; Andersen, J. N. *Surf. Sci.* **2000**, *470*, 171.
(17) Kohn, W.; Sham, L. *Phys. Rev.* **1965**, *140*, A1133.
(18) Jones, R. O.; Gunnarsson, O. *Rev. Mod. Phys.* **1989**, *61*, 689.
(19) Car, R.; Parrinello, M. *Phys. Rev. Lett.* **1985**, *55*, 2471.
(20) Payne, M. C.; Teter, M. P.; Allan, D. C.; Arias, T. A.; Joannopoulos, J. D. *Rev. Mod. Phys.* **1992**, *64*, 1045.
(21) Kresse, G.; Surnev, S.; Ramsey, M. G.; Netzer, F. P. *Surf. Sci.* **2001**,*492*, 329.
(22) Kresse, G.; Hafner, J. *Phys. Rev. B* **1993**, *48*, 13115.
(23) Kresse, G.; Furthmüller, J. *Comput. Mater. Sci.* **1996**, *6*, 15. Kresse, G.; Furthmüller, J. *Phys. Rev. B* **1996**, *54*, 11169.
(24) Blöchl, P. E. *Phys. Rev. B* **1994**, *50*, 17953.
(25) Kresse, G.; Joubert, D. *Phys. Rev. B* **1999**, *59*, 1758.
(26) Wang, Y.; Perdew, J. P. *Phys. Rev. B* **1991**, *44*, 13298.
(27) Perdew, J. P.; Chevary, J. A.; Vosko, S. H.; Jackson, K. A.; Pederson, M. R.; Singh, D. J.; Fiolhais, C. *Phys. Rev. B* **1992**, *46*, 6671.
(28) Köhler, L.; Kresse, G. To be published.
(29) Tersoff, J.; Haman, D. R. *Phys. Rev. B* **1985**, *31*, 805.
(30) Andersen, J. N.; Henning, D.; Lundgren, E.; Methfessel, M.; Nyholm, R.; Scheffler, M. *Phys. Rev. B* **1994**, *50*, 17525.
(31) Steltenpohl, A.; Memmel, N. *Surf. Sci.* **1999**, *443*, 13.
(32) Hayek, K.; Jenewein, B.; Klötzer, B.; Reichl, B. *Top. Catal.* **2001**, *14*, 25.
(33) Klötzer, B.; Hayek, K. Private communication.
(34) Sock, M.; Surnev, S.; Andersen, J. N.; Ramsey, M. G.; Netzer, F. P. in preparation.
(35) Reuter, K.; Scheffler, M. *Phys. Rev. B* **2002**, 65, 035406.